Biosensors and Bioelectronics 79 (2016) 41–47

Contents lists available at ScienceDirect

Biosensors and Bioelectronics

journal homepage: www.elsevier.com/locate/bios

Determination of cell metabolite $VEGF_{165}$ and dynamic analysis of protein–DNA interactions by combination of microfluidic technique and luminescent switch-on probe

Xuexia Lin [a,b,c,1], Ka-Ho Leung [c,1], Ling Lin [a], Luyao Lin [a], Sheng Lin [c], Chung-Hang Leung [d], Dik-Lung Ma [c,*], Jin-Ming Lin [a,*]

[a] Department of Chemistry, Beijing Key Laboratory of Microanalytical Methods and Instrumentation, The Key Laboratory of Bioorganic Phosphorus Chemistry & Chemical Biology, Tsinghua University, Beijing 100084, China
[b] College of Chemical Engineering, Huaqiao University, Xiamen 361000, China
[c] Department of Chemistry, Hong Kong Baptist University, Kowloon Tong, Hong Kong, China
[d] State Key Laboratory of Quality Research in Chinese Medicine, Institute of Chinese Medical Sciences, University of Macau, Macao, China

ARTICLE INFO

Article history:
Received 8 August 2015
Received in revised form
1 November 2015
Accepted 28 November 2015
Available online 30 November 2015

Keywords:
$VEGF_{165}$
Kinetic analysis
Microfluidic device
Iridium (III) probe
Functional nucleic acid

ABSTRACT

In this paper, we rationally design a novel G-quadruplex-selective luminescent iridium (III) complex for rapid detection of oligonucleotide and $VEGF_{165}$ in microfluidics. This new probe is applied as a convenient biosensor for label-free quantitative analysis of $VEGF_{165}$ protein from cell metabolism, as well as for studying the kinetics of the aptamer–protein interaction combination with a microfluidic platform. As a result, we have successfully established a quantitative analysis of $VEGF_{165}$ from cell metabolism. Furthermore, based on the principles of hydrodynamic focusing and diffusive mixing, different transient states during kinetics process were monitored and recorded. Thus, the combination of microfluidic technique and G-quadruplex luminescent probe will be potentially applied in the studies of intramolecular interactions and molecule recognition in the future.

1. Introduction

Proteins serve as the molecular “workers” of cells that play important roles for carrying signals, chemical messengers, and regulating the functions in cells. Detection and quantification of proteins during cellular metabolism will be beneficial to understand the cell culture conditions and reflect the resultant effects on the productions (Burleigh et al., 2011; Cairns et al., 2011; Gambhir et al., 2003), which will promote the understanding of cancer disease-related biological processes (Ghesquière et al., 2014; Jain et al., 2012; Oladipupo et al., 2011; Papadopoulos et al., 2012), and also reveal the intracellular biochemical reaction rates (DeBerardinis and Thompson 2012; Paige et al., 2012; Wu et al., 2013; Papadopoulos et al., 2012). Recently, in-depth insights into cell metabolism become an important tool in the disease-marker discovery in the basic and applied biomedical researches (Chen et al., 2012; Xu et al., 2014; Ning et al., 2014). In general, traditional approaches for the determination of protein and nucleic acid interactions are commonly implemented by gel retardation, DNASE1 foot-printing, methylation interference, chromatin immune precipitation. Most of them are tedious, time-consuming, and high cost. An efficient and simple strategy for rapid and sensitive detection of cancer-related proteins is, thus, an urgently required.

Nucleic acid aptamers are single-stranded oligonucleotides from DNA/RNA libraries, which can bind specific molecular targets (Freeman et al., 2012; Iliuk et al., 2011). Due to their high affinity and specificity, aptamers have been most widely used for disease diagnosis, cell therapy, drug delivery and biosensors. More importantly, functional nucleic acid (FNA), which is aptamer assembled with DNAzyme (Aleman-Garcia et al., 2014; Nakayama and Sintim 2009) is available for catalyzing chemical reactions by binding the targets. Meanwhile, because the long-lived phosphorescence allowing for distinguishing fluorescent environment, large Stokes shifts can reduce self-quenching, and modular synthesis that can easily change the photophysical and molecular recognition properties without labour-intensive synthetic protocols (Leung et al., 2013; Ma et al., 2014), photoluminescent iridium (III) complex has attracted more and more interests in luminescence signaling and sensory applications. We report herein the synthesis and application of a novel G-quadruplex-selective

* Corresponding authors.
E-mail addresses: edmondma@hkbu.edu.hk (D.-L. Ma), jmlin@mail.tsinghua.edu.cn (J.-M. Lin).
[1] These authors contributed equally.

http://dx.doi.org/10.1016/j.bios.2015.11.089
0956-5663/

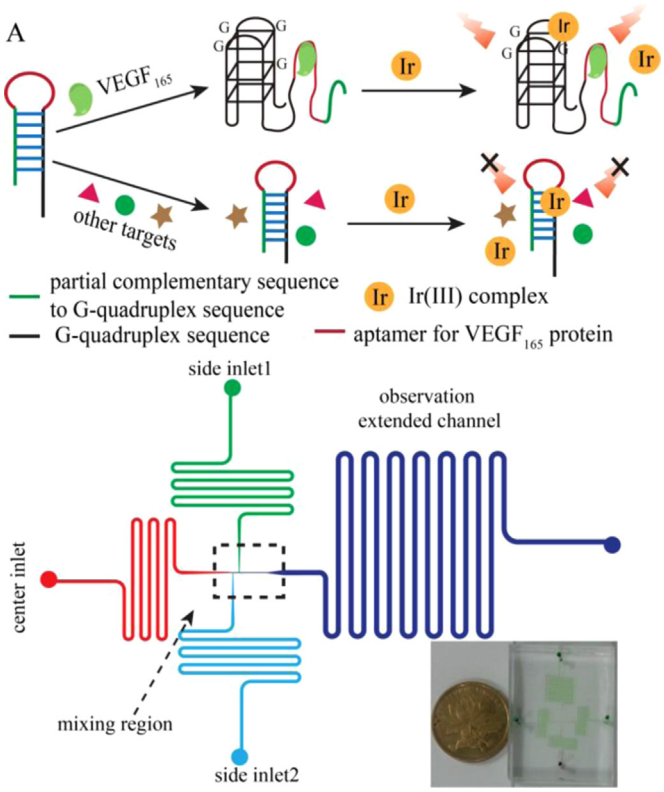

Fig. 1. G-quadruplex probe **1** for $VEGF_{165}$ assay in the microchip. (A) Schematic illustration of $VEGF_{165}$ assay based on G-quadruplex probe **1**. (B) The profile of microfluidic mixing device. The center inlet was applied to introduce $VEGF_{165}$ solution. The side inlet2 was used to introduce DNA solution, while complex **1** was injected from side inlet1. Solutions can be rapidly mixed in the mixing region. Extended observing channel prolongs the observation time up to minutes.

luminescent iridium (III) complex **1** for label-free, rapid and sensitive determination of $VEGF_{165}$ from cell metabolite. The mechanism of this assay is illustrated in Fig. 1, and the structure of iridium (III) complex **1** in Fig. 2A. Nowadays, quantitative investigation of the interplay of protein and nucleic acid shows great promises for revealing the potential mechanism of cellular signaling process. For example, quantitative investigation of the interplay of protein and nucleic acid shows great promises for revealing the potential mechanism of cellular signaling process. For these reasons, monitoring the interactions of protein and nucleic acid will facilitate to understand the dynamic equilibrium of protein-nucleic acid complex or protein folding pathways, and to elucidate the transitions occurring between different conformational states (Hwang and Myong 2014; Konishi et al., 2012; Schuler and Hofmann 2013). Meanwhile, because protein-nucleic acid interaction occurs at the moment when protein molecules promote a DNA/RNA conformational transition (Hofmann, et al., 2010; Lipman et al., 2003), dynamic resolution of the instruments is required on milli-/micro- second scale resolution (Vahidi, et al., 2013; Zhang et al., 2014). It is a huge challenge by the existing method. Recently, microfluidic mixing is emerged as an excellent method for observing transient states of protein and nucleic acid complexes (Gambin, et al., 2010; Johnson, et al., 2002; Xia, et al., 2005; Wunderlich et al., 2013) due to the following advantages: (i) eliminating turbulence and enhancing laminar and steady fluid flow in microchannel, providing the possibility of building a mathematical model for complex geometries; (ii) precisely controlling flow rates at a short diffusion time allows them to achieve the accurate results within milli-/micro-second scale and little effect on surrounding environments; (iii) easily recording the reaction process by emplacing different observation positions along the microchannel; (IV) only an extremely small sample volume (microliters) is required for each assay, resulting in minimizing reagent and sample consumption. However, despite its high scale resolution and its broad dynamic range, the stability of the system is limited especially in the multiplex inlets. In this context, the U sharp channels are designed at nearby the inlets. The adding U-sharp channels alter the pressure of the system, resulting in greatly improving the stability of the system.

Vascular endothelial growth factor ($VEGF_{165}$), a kind of glycolated protein, is a crucial angiogenic mitogen over-expressed in the tumor cells, and can induce their migration, excessive proliferation, invasion and metabolism in the body (Choi et al., 2013; McCarthy, 2012; Saharinen et al., 2011). Moreover, various kinds of $VEGF_{165}$ aptasensor have been developed (Cho et al., 2012; Freeman et al., 2012; Iliuk et al., 2011; Kwon et al., 2012). As a proof-of-concept, $VEGF_{165}$ is selected as a model analyte of glycolated protein. The cell metabolite $VEGF_{165}$ was analyzed based on a new synthesized iridium (III) complex and a fragment of FNA. The iridium (III) complex was a G-quadruplex-selective luminescent probe. The FNA fragment is hairpin structure including $VEGF_{165}$ aptamer, G-quadruplex sequence and its complementary sequence. The usage of this aptasensor can specifically detect $VEGF_{165}$ with low background because the hairpin structure cannot bind to iridium (III) complex, and hairpin structure of fragment is not easy to degrade. The high luminescent signal can be only recorded when it is in the present of $VEGF_{165}$ because the hairpin structure was destroyed. Furthermore, we designed a microfluidic device for monitoring protein–nucleic acid interactions. The application of U-sharp channels greatly improve the stability in the system, and the frequency of every transients can be recorded combination with iridium (III) complex 1. The results showed that our designed device can not only provide a highly sensitive system for kinetic study of protein-DNA complexes especially in cases where reagents or samples are in limited supply, but also for cell metabolites analysis.

2. Experimental section

2.1. Cell culture

CaSki cell line was purchased from Cancer Institute & Hospital Chinese Academy of Medical Science (Beijing, China). CaSki cells were cultured in DMEM media supplemented with 1% fetal bovine serum (FBS), 100 μg/mL penicillin, and 100 μg/mL streptomycin. CaSki cells were also cultured with the final concentration 10 μg/mL of paclitaxel. Cells were maintained in a humidified atmosphere with 5% CO_2 at 37 °C.

2.2. Iridium complex 1 synthesis

The complex **1** were prepared according to literature methods (Ma et al., 2014), but the ligand is different. All complexes are characterized by ^{1}H NMR, ^{13}C NMR and high resolution mass spectrometry (HRMS). Complex **1**. Yield: 57%. ^{1}H NMR (400 MHz, Acetone-d_6) δ 8.44–8.42 (d, J=8.0 Hz, 2H), 8.15 (s, 2H), 8.09–8.05 (m, 4H), 7.88 (s, 2H), 7.64 (s, 10H), 7.18–7.14 (t, J=8.0 Hz, 2H), 6.76-6.70 (t, J=8.0 Hz, 2H), 5.78-5.76 (d, J=8.0 Hz, 2H),2.38 (s, 6H); ^{13}C NMR (400 MHz, Acetone-d6) δ 164.8, 164.0, 163.9, 161.4, 159.8, 153.7, 153.6, 151.2, 150.9, 148.6, 139.7, 135.8, 129.7, 129.6, 129.0, 128.5, 128.0, 127.8, 125.0, 123.8, 123.7, 123.5, 113.7, 113.5, 98.6, 98.3, 98.1, 27.2; HRMS: Calcd. for $C_{48}H_{32}F_4IrN_4$ $[M–PF_6]^+$: 933.2192, found: 933.2224; elemental anal. ($C_{48}H_{32}N_4IrPF_{10}$) C, H, N: calcd: 53.48, 2.99, 5.2; found: 53.23, 3.07, 5.25.

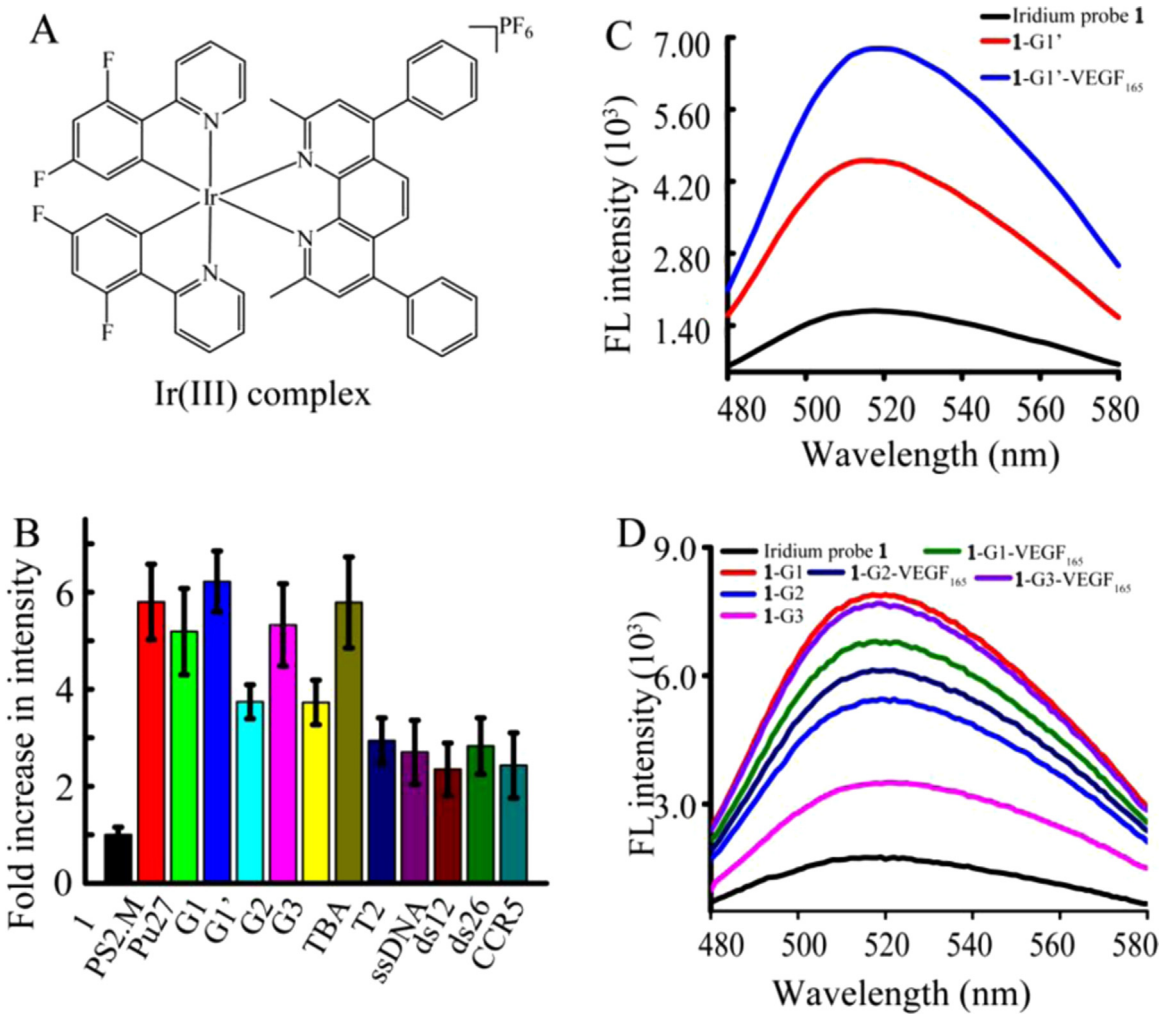

Fig. 2. The selectivity of iridium complex **1**. (A) The structure of iridium complex **1**. (B) The fold increase in luminescence emission of **1** with different kinds of DNA; (C) The luminescence intensity of **1** bind to G1′. (D). The luminescence intensity of **1** bind to G1, G2, G3, respectively. The concentration of **1** was 4.00 μM. The concentrations of various kinds of DNA were 5.00 μM.

2.3. Single-molecule spectroscopy for $VEGF_{165}$ assay

Complex **1** (excitation, 310 nm; emission, 516 nm), oligonucleotide solution and $VEGF_{165}$ were introduced into the channel by a Harvard pump (PHD 2000 programmable). A fluorescence microscope (Leica DMI 4000B, Wetzlar, Germany) was used to acquire single molecule luminescence spectra data, and a CCD camera was equipped to obtain image and movie of the microfluidic devices. Signals generated under a 310 nm laser excitation and were collected by a CCD camera. These data were reorganized to give luminescence intensity time trajectories of individual molecules. The luminescence intensities were binned and fitted to four Gaussian distributions respectively, representing intensities of the complex **1** only, **1** with DNA, **1** with $VEGF_{165}$ and **1**-DNA with protein bound. Relative frequency analysis was conducted to determine the sensitivity in each structural change event. Moreover, data of time dependent-luminescent intensity were also recorded by fluorescence spectrophotometer (Hitachi F-7000), with time resolution of 0.002 s.

3. Results and discussion

3.1. Oligonucleotides and switch-on iridium (III) probe for $VEGF_{165}$ assay

The G-quadruplex is a DNA/RNA secondary structure formed by guanine-rich sequences, and consists of square-planar arrangements of guanine nucleobases stabilized by Hoogsteen hydrogen bonding and monovalent cations (Davis 2004; Ma et al., 2008). In this work, we hypothesis that aptamer of $VEGF_{165}$, G-quadruplex and its complementary sequence can form the stable hairpin structure. The aptamer sequence of $VEGF_{165}$ would be in loop area. In the presence of $VEGF_{165}$, the hairpin DNA was opened, and G-quadruplex structure would be formed. Then the special Irdium complex **1** would bind to G-quadruplex structure and generate to strong luminescence. In the absence of $VEGF_{165}$, hairpin structure can not be opend, resulting in weak luminescence in Fig. 1A. Therefore, different oligonucleotide sequences (G1, G2, G3 and G1′) were designed in Table S1. The selectivity of luminescent iridium (III) complex **1** was confirmed by different kinds of oligonucleotides including double-stranded DNA, single-stranded DNA, and various G-quadruplex DNA in Fig. 2B. It was found that iridium (III) complex **1** can selectively recognize G-quadruplex structures such as PS2.M and Pu27, resulting in strong luminescence at 520 nm. On the other hand, complex **1** had low background luminescent signal in buffer solution (100 mM Tris–HCl, 150 mM KCl, pH 8.0) or in the presence of single-stranded DNA (ssDNA) or double-stranded DNA (dsDNA). Absorption spectra of 2 μM

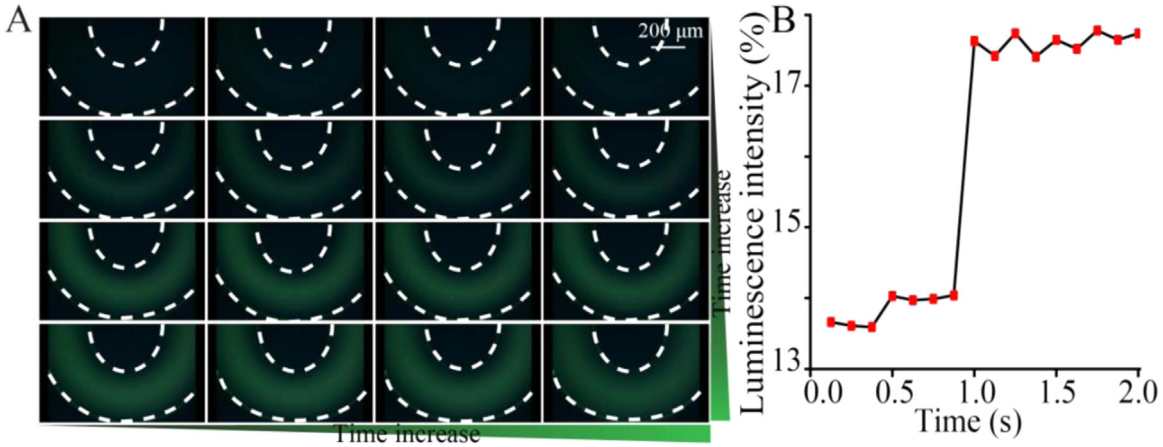

Fig. 3. (A) At turning 3, time dependent- luminescence images of sample traces representing the interaction among $VEGF_{165}$, DNA and **1**. The time set as zero when the samples were beginning to meet. When the solutions begin to meet, the pump was powered off on instant. Picture was taken every 0.125 s. (B) The time-dependent intensity during 2 s after mixing $VEGF_{165}$, DNA, and **1**.

complex **1** in acetonitrile were showed in Fig. S1. Interestingly, the emission wavelength of **1** was observed to shift to 516 nm when the complex flowed into a microchannel, with its intensity greatly decreased, which was attributed to the absorption of luminescence by PDMS in Fig. S2.

In absence of $VEGF_{165}$, the signals of G1, TBA and PS2.M were highest, and then PU27 and G2, indicating that G1 and G2 may initially exist as G-quadruplex structures because all of these oligonucleotide contained G-quadruplex sequence. And PS2.M, Pu27, and TBA have been well proved to be G-quadruplex (Fig. 2B). In the presence of 13.00 nM $VEGF_{165}$, the intensities of G1 and G2 were weak, demonstrating the failed designing of G1 and G2 oligonucleotides (Fig. 2D). Fig. 2C showed that in the presence of $VEGF_{165}$, the intensity was greatly increased by the application of G1′ and **1**, indicating that G1′ can be used for $VEGF_{165}$ assay. Meanwhile, the intensity of G3 was lower in the absence of $VEGF_{165}$, but was greatly enhanced upon the addition of oligonucleotide. These results showed that G3 would also be suitable to $VEGF_{165}$ assay. In applying G1′ and G3 to detect $VEGF_{165}$, we found the limit of detection (LOD) of G1′ was lower than that of G3 (Fig. S3), therefore, G1′ was applied in the following experiments. Furthermore, the concentration of **1** was optimized, and the control experiment was performed in the absence of the correspondent concentration of $VEGF_{165}$. We found that 3.00 μM of **1** gave a lower background signal and a wider linear range comparing with 4.00 μM and 5.00 μM of **1** (Fig. S4). Thus, 3.00 μM of **1** was used for the $VEGF_{165}$ assay.

3.2. Design of microfluidic device for $VEGF_{165}$ assay

Our microfluidic device allows the entire changes of protein–induced DNA interactions to be monitored, and intermediates detected, which was manufactured by standard soft-lithography technology in Fig. S5 (Lin et al., 2014; Wang et al., 2014). By controlling the flow rate, we ensured that the initiation for DNA folding observation was completed before the earliest change in DNA or protein conformation began. Fig. 1B presents the layout and key elements of the device (the details was provided in supporting information 3.1 part and Fig. S6). Fig. S6B shows mixing channel with 40 μm width allowing for rapid samples exchange. The resolution time between adjacent collection points in our device is 1.0 ms, which is enough for study the interaction of protein and DNA (Gambin et al., 2011). Furthermore, the concentration of DNA was optimized in Fig. S7 (the details provide in the Supporting information Part 3.3), the time required for mixing can be accurately calculated at different observation position, and was simulation on COMSOL in Fig. S8. The details were provided in 3.2 part of Supporting information.

The little changes of flow rate would affect the interaction rate of protein and DNA. Thus, the stability of flow rate was studied. The stability of flow rate depended on the fabrication of microchip and the precision of pump. The rate of transporting the solution to the microchip relied on the precision of pump. Furthermore, the fabrication of microchip mainly affects on the channel pressure (Pa), and then influenced the fluctuation of flow rate. Highly precise pump and the short U-sharp channels were applied. Very little changes of the flow rate in the system under different inlet velocities from 0.5 μL/min to 20 μL/min were observed in Fig. S9, all of the deviation of the measured flow rate was lower than 0.05% ($n=3$), indicating that the designed microdevice is suitable for the investigation of protein and DNA interplay. To further study the effect of flow rate on mixing and reaction efficiency, 10.00 pM $VEGF_{165}$, 5.00 μM DNA, and 3.00 μM complex **1** were diluted in the red, green, and blue dyes separately to mimic the protein-DNA reaction. Fig. S10 shows at turning 1 and 2, the color in the middle of channel is deeper than that in the edges, indicating that the reaction would firstly accomplish in the middle, but not complete in the edges of channel. But the color was uniformed at the turning 5 with 1 μL/min infusion rate. However, there were still some color differences at the turning 7 with 2 μL/min infusion rate. The results demonstrated that flow rate is a major factor influencing the rate of $VEGF_{165}$ and DNA reaction because the flow rate affects the solution diffusion rate and the mixing speed. And a low flow rate will improve reaction efficiency. The application of 1 μL/min for following experiments was determined by the shortest travel distance in channel for a complete reaction. More details were provided in Supporting information 3.3 parts.

3.3. Kinetic study of protein-DNA

We investigate the dynamics interaction of $VEGF_{165}$ and DNA by single-molecule instrument (FV1200 laser scanning microscope, Olympus, Japan), with the data processing as well as generation of corrected transfer efficiency histograms by fluoview ASW 4.0 software. When the solutions began to meet, we set the time as 0 s. And the same moment we powered off the pump on instant to collect the data. In order to monitor the interaction procedure, the observation position was set at turning 3, and the observation time was extended to 2 s. As shown in Fig. 3, the signal was barely increased from 0.375 s to 0.500 s, representing that $VEGF_{165}$ had bonded to a portion of one DNA chain. Then, $VEGF_{165}$ would slide to a particular space of DNA (0.500–1.000 s),

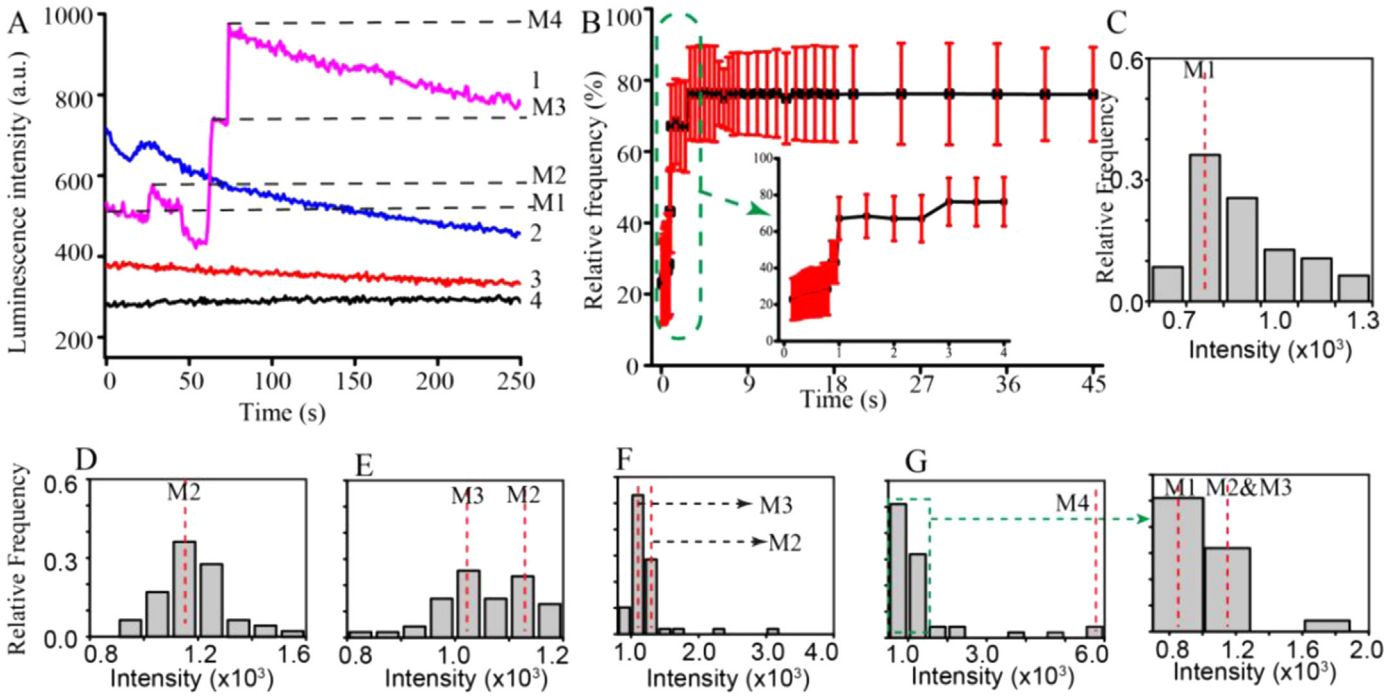

Fig. 4. The kinetic study of protein-DNA interaction. (A) The luminescence spectrum of $VEGF_{165}$, DNA and complex **1** during 250 s. (B) The relative frequency of **1**, $VEGF_{165}$ and DNA complex against time. (C) and (D) represent transfer efficiency histograms at turning 3 for the time of 0.250 s, and 0.375 s, respectively. (E), (F), and (G) represent transfer efficiency histograms at turning 3, turning 4, turning 5 for the time of 0.500 s, respectively. 1: among $VEGF_{165}$, DNA, and **1**; 2: between DNA and complex **1**; 3: between **1** and $VEGF_{165}$; 4: only complex **1**. M1: complex **1**; M2: the **1** and $VEGF_{165}$ complex; M3: the **1** and DNA complex; M4: **1**, $VEGF_{165}$ and DNA complex. Every point was tested three times. Precise positioning of laser focus was limited by minimal movement of 0.5 μm in microscopy platform.

open the hairpin structure, and form the G-quadruplex, inducing iridium complex bond to G-quadruplex, resulting in high intensity (1.000 s). When the time was extended to 2.00 s, the whole channel was fulfilled with protein-DNA complex. When the luminescence in Fig. 3A was translated to the intensity, the intensity was greatly increased at 1.000 s, indicating the quantum jumps happened. In order to further study the kinetics of $VEGF_{165}$ and DNA, the relative frequencies of them were analyzed by transfer efficiency histograms (Wunderlich et al., 2013). They show the intensity of **1**, **1** and DNA complex, **1** and $VEGF_{165}$ complex, and **1**, DNA and $VEGF_{165}$ complex were corresponding to $I=0.8\times10^4$, $I=1.12\times10^4$, $I=1.01\times10^4$, and $I=5.8\times10^4$, respectively (Fig. 4C–G). Furthermore, it also shows the proportion of populations (relative frequency) was changed depending on the time and the position. When the observation location was fixed at turning 3, the luminescence was mainly depending on complex **1** at 0.250 s (Fig. 4C), while it was mainly **1** and $VEGF_{165}$ complex (Fig. 4D) at 0.375 s, suggesting temporal varied dynamics. When the time was fixed at 0.500 s, the relative frequencies of different observation points were analyzed. **1** and $VEGF_{165}$ complex appeared at turning 4 and increased at turning 5 (Fig. 4F and G). The **1**, DNA and $VEGF_{165}$ complex appeared at turning 5, but it cannot be observed at turning 3 and 4. These results showed that the time and the distance affected sample mixing and then influenced the interaction between $VEGF_{165}$ and DNA.

To study the interaction of the **1**, DNA and $VEGF_{165}$ complex, the time was extended to 45 s at turning 3. From Fig. 4B, the frequency was slowly increased during 1.0 s, and greatly enhanced at 1.0 s, and then maintained till 3 s. This is consistent with the Fig. 3, which explained the luminescence enhancement. However, the luminescence was enhanced again at 3.0 s, indicating that $VEGF_{165}$ bond to DNA completely and formed G quadruplex at 1.0 s, and the reaction reached equilibrium. The images of **1**-DNA and **1**-DNA-$VEGF_{165}$ showed that their intensity was greatly changed during 3 s mixing in Fig. S11. This implied that $VEGF_{165}$ induced changes of DNA conformation, causing luminescence signal enhancement. These results demonstrated our designed device can be applied to study the interaction between protein and DNA. It also suggested that our hypothesis of $VEGF_{165}$ assay based on DNA is feasible. To further understand the kinetics profile, the luminescence spectra for the interplay between protein and DNA was detected by fluorescence spectrophotometer at turning 3 in Fig. 4A. The populations of complex **1**, **1** and DNA complex, **1** and $VEGF_{165}$ complex, and **1**, DNA and $VEGF_{165}$ complex were found in one test, suggesting that the interaction happened among complex **1**, DNA, and $VEGF_{165}$, which confirmed the kinetics study in the single molecule level in Figs. 3 and 4B–G.

3.4. *Specificity, sensitivity and recovery*

From the kinetic analysis of $VEGF_{165}$ and the hairpin structure DNA, we found that the DNA can be applied to analyze $VEGF_{165}$ protein from complex matrix. Then, the specificity of the system was investigated by the influence of various proteins. 5.00 μM DNA with 3.00 μM complex **1** and different target species were investigated. Fig. 5A shows that the luminescence response of the system to $VEGF_{165}$ (26.00 pM) was over ten-fold stronger than those to other proteins and molecules including immunoglobulin G (IgG), concanavalin A (Con. A), adenosine triphosphate (ATP), bovine serum albumin (BSA), thrombin, platelet-derived growth factor-BB (PDGF-BB) and ascorbic acid (260.00 pM). It demonstrated that G1′ has an excellent selectivity for $VEGF_{165}$.

The quantitative analysis was assessed by the luminescence intensity of targets with different concentrations of $VEGF_{165}$ protein (0.00, 0.52, 5.20, 13.00, 26.00, 52.00, 65.00, 78.00 pM). As shown in Fig. 5B, there was a good linear correlation of $y=68.03x+5041.53$ ($R^2=0.983$) in the range from 0.52 to 52.00 pM with low relative standard deviations (RSDs) between 2.9% and 6.3% ($n=3$). By calculation of signal to noise ratio at 3, the limit of detection was 0.17 pM (~6.50 pg/mL, the molecular

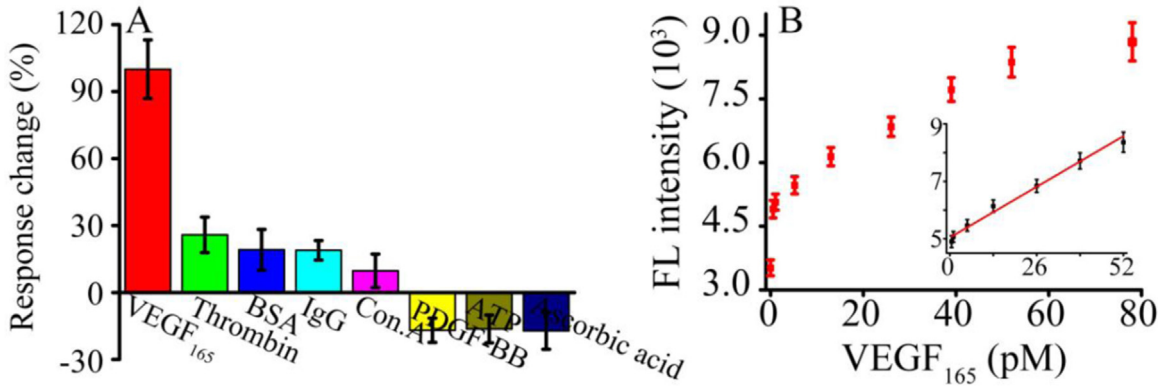

Fig. 5. Analysis of $VEGF_{165}$ based on DNA G1′ and complex **1**. (A) The selectivity of the system. The system contained 3.00 μM **1**, 5.00 μM DNA, 26.00 nM $VEGF_{165}$, while interfering species were set at 260.00 nM. (B) The linear range of the system from 0.52 nM to 78.0 nM. The system included 3.00 μM **1**, 5.00 μM DNA, and several concentration of $VEGF_{165}$. The linear equation was $y=68.03x+5041.53$ ($R^2=0.983$). The LOD was calculated by3 fold of the ratio for signal to noise.

Table 1
Recovery of VEGF165 in cell medium.

Conc. (pM)	I/I_0	Standard I/I_0	Recovery (%)	RSD
0.52	1.15	1.09	106.24	0.02
5.20	1.51	1.41	106.81	0.10
13.00	1.82	1.64	111.09	0.03
26.00	2.08	2.35	88.58	0.01
52.00	2.56	3.19	80.28	0.37

weight of $VEGF_{165}$ is ~38.2 KD). The sensitivity of the proposed method may be suitable for analyzing cell secretion because the concentration of $VEGF_{165}$ in common cell medium was about 1.0 ng/mL. To mimic real samples and assess the accuracy of established method by the recovery, various concentrations of $VEGF_{165}$ were spiked into DMEM cell medium by the standard addition method and were determined by the established method in Table 1. The recoveries of VEGF165 from cell secretions ranged from 80.28% to 111.1% with the RSDs between 0.02% and 3.76% ($n=3$), indicating that the established method can be applied for $VEGF_{165}$ from complex matrix.

3.5. Real sample analysis

The DMEM cell medium and cell medium with pacilitaxel were used to culture CaSki cells, respectively. Then, cell medium was collected every 24 h for analyzing metabolites $VEGF_{165}$ protein. As shown in Fig. 6A, the concentrations of $VEGF_{165}$ ranged from 8.32 pM to 13.11 pM (320.00–504.23 pg/mL) for cell cultured without paclitaxel, and 7.62 pM to 10.67 pM (293.07–410.38 pg/mL) for cell cultured with the finally concentration 10 μg/mL paclitaxel, which indicated that the established method could monitor cell secretions. Furthermore, the concentrations of $VEGF_{165}$ were increased with increasing time with culture medium without paclitaxel, and the concentrations of $VEGF_{165}$ were gradually decreased with increasing time by paclitaxel effects. These results demonstrated that paclitaxel was useful for inhibition of the secretion $VEGF_{165}$ of tumor cell, which were consistent with

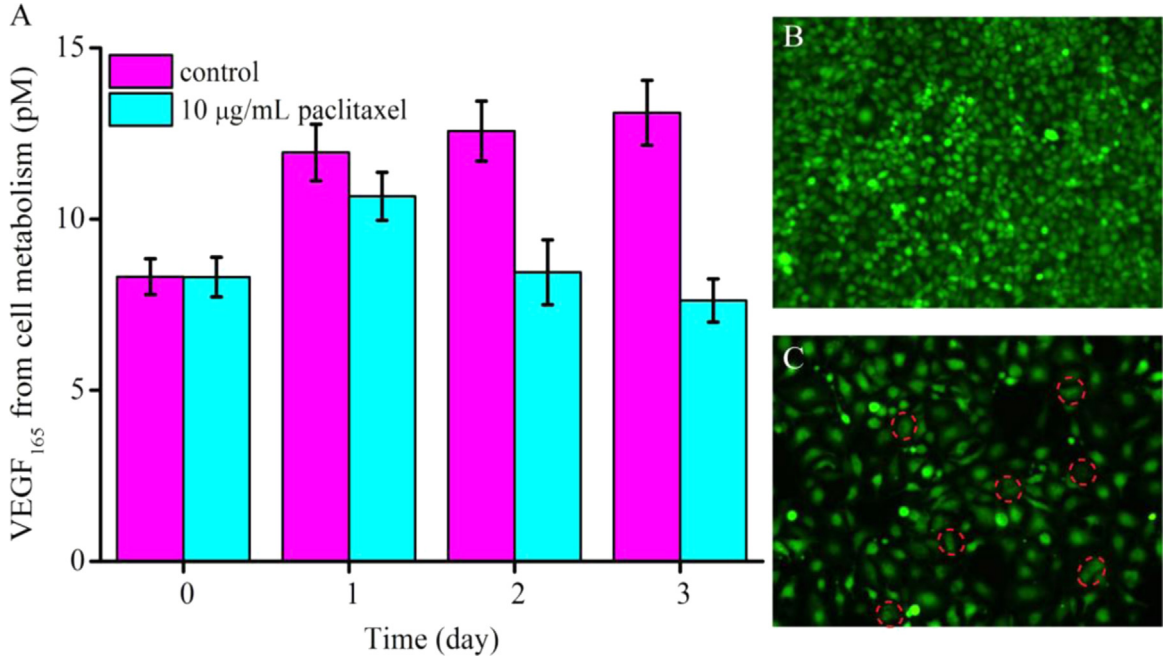

Fig. 6. Analysis of $VEGF_{165}$ from cell medium with paclitaxel. (A) Analysis of $VEGF_{165}$ from cell medium. (B) CaSki cells cultured in DMED medium without paclitaxel.(C) CaSki cells cultured in DMED medium with 10 μg/mL paclitaxel. Control was set as cell medium contained 1% FBS without paclitaxel. 10 μg/mL paclitaxel was cell medium contained 1% FBS and 10 μg/mL paclitaxel. The red dashed area displayed the damage of cell microtubules by 10 μg/mL paclitaxel. (For interpretation of the references to color in this figure legend, the reader is referred to the web version of this article.)

the reports. These results may be due to that paclitaxel is a mitotic inhibitor that stabilizes cellular microtubules, and interferes with the normal breakdown of microtubules in Fig. 6B. Thus, paclitaxel inhibits tumor cell to secret $VEGF_{165}$ protein. All of $VEGF_{165}$ protein detection was confirmed by ELISA kit from R&D system, Inc. (USA). The LOD and the linearity range of the established method were comparable to those of the ELISA assay in Fig. S12 although the intensities ratio from the developed method were over than those from ELISA. We deduced that the higher intensity ratio of the established method may be due to iridium (III) complex itself has a certain luminescence, but ELISA detection has no such luminescence.

4. Conclusions

In summary, the G-quadruplex specific probe complex **1** (iridium (III) complex **1**) has been successfully developed to achieve dynamically monitoring DNA and $VEGF_{165}$ protein interactions from milliseconds to minutes on the microfluidic device. For data analysis, a comprehensive profile of the reaction transfer was demonstrated by photon counting histograms, luminescence life spectrum, and correlation analysis. In the kinetic analysis, the profile of DNA and protein interaction was also provided, and the quantitative analysis of cell secreted $VEGF_{165}$ was achieved. Consequently, we hopefully anticipate that this designed device and G-quadruplex-selective luminescent iridium (III) complex will find more applications in resolving questions concerning complex mechanisms in biomolecular reactions, and can be applied to other cancer related-protein analysis.

Notes

The authors declare no competing financial interest.

Acknowledgments

This work was supported by National Natural Science Foundation of China (Nos. 81373373, 21435002 and 91213305), the French National Research Agency/Research Grants Council Joint Research Scheme (A-HKBU201/12) and the Science and Technology Development Fund, Macao SAR (103/2012/A3).

Appendix A. Supplementary material

Supplementary data associated with this article can be found in the online version at http://dx.doi.org/10.1016/j.bios.2015.11.089.

References

Aleman-Garcia, M.A., Orbach, R., Willner, I., 2014. Chem.: Eur. J. 20, 5619–5624.
Burleigh, S.C., van de Laar, T., Stroop, C.J.M., van Grunsven, W.M.J., O'Donoghue, N., Rudd, P.M., Davey, G.P., 2011. BMC Biotechnol. 11, 95.
Cairns, R.A., Harris, I.S., Mak, T.W., 2011. Nat. Rev. Cancer 11, 85–95.
Chen, Q., Wu, J., Zhang, Y., Lin, J.-M., 2012. Anal. Chem. 84, 1695–1701.
Cho, H., Yeh, E.-C., Sinha, R., Laurence, T.A., Bearinger, J.P., Lee, L.P., 2012. ACS Nano 6, 7607–7614.
Choi, D.H., Subbiah, R., Kim, I.H., Han, D.K., Park, K., 2013. Small 9, 3468–3476.
Davis, J.T., 2004. Angew. Chem. Int. Ed. 43, 668–698.
DeBerardinis, R.J., Thompson, C.B., 2012. Cell 148, 1132–1144.
Freeman, R., Girsh, J., Fang-ju, A., Ho, J.-A., Hug, T., Dernedde, J., Willner, I., 2012. Anal. Chem. 84, 6192–6198.
Gambhir, A., Korke, R., Lee, J., Fu, P.C., Europa, A., Hu, W.S., 2003. Biosci. Bioeng. 95, 317–327.
Gambin, Y., Simonnet, C., VanDelinder, V., Deniz, A., Groisman, A., 2010. Lab Chip 10, 598–609.
Gambin, Y., VanDelinder, V., Ferreon, A.C.M., Lemke, E.A., Groisman, A., Deniz, A.A., 2011. Nat. Methods 8, 239–244.
Ghesquière, B., Wong, B.W., Kuchnio, A., Carmeliet, P., 2014. Nature 511, 167–176.
Hwang, H., Myong, S., 2014. Chem. Soc. Rev. 43, 1221–1229.
Hofmann, H., Hillger, F., Pfeil, S.H., Hoffmann, A., Streich, D., Haenni, D., Nettels, D., Lipman, E.A., Schuler, B., 2010. Proc. Natl. Acad. Sci. USA 107, 11793–11798.
Iliuk, A.B., Hu, L., Tao, W.A., 2011. Anal. Chem. 83, 4440–4452.
Jain, M., Nilsson, R., Sharma, S., Madhusudhan, N., Kitami, T., Souza, A.L., Kafri, R., Kirschner, M.W., Clish, C.B., Mootha, V.K., 2012. Science 336, 1040–1044.
Johnson, T.J., Ross, D., Locascio, L.E., 2002. Anal. Chem. 74, 45–51.
Leung, K.-H., He, H.-Z., Ma, V.P.-Y., Zhong, H.-J., Chan, D.S.-H., Zhou, J., Mergny, J.-L., Leung, C.-H., Ma, D.-L., 2013. Chem. Commun. 49, 5630–5632.
Lin, X., Chen, Q., Liu, W., Li, H., Lin, J.-M., 2014. Biosens. Bioelectron. 56, 71–76.
Lipman, E.A., Schuler, B., Bakajin, O., Eaton, W.A., 2003. Science 301, 1233–1235.
Konishi, T., Kiguchi, M., Takase, M., Nagasawa, F., Nabika, H., Ikeda, K., Uosaki, K., Ueno, K., Misawa, H., Murakoshi, K., 2012. J. Am. Chem. Soc. 135, 1009–1014.
Kwon, O.S., Park, S.J., Hong, J.-Y., Han, A.-R., Lee, J.S., Lee, J.S., et al., 2012. ACS Nano 6, 1486–1493.
Ma, D.-L., Lin, S., Leung, K.-H., Zhong, H.-J., Liu, L.-J., Chan, D.S.-H., Bourdoncle, A., Mergny, J.-L., Wang, H.-M.D., Leung, C.-H., 2014. Nanoscale 6, 8489–8494.
Ma, D.-L., Wong, W.-L., Chung, W.-H., Chan, F.-Y., So, P.-K., Lai, T.-S., Zhou, Z.-Y., Leung, Y.-C., Wong, K.-Y., 2008. Angew. Chem. Int. Ed. 47, 3735–3739.
McCarthy, N., 2012. Nat. Rev. Cancer 12, 581.
Nakayama, S., Sintim, H.O., 2009. J. Am. Chem. Soc. 131, 10320–10333.
Ning, R., Wang, S., Wu, J., Wang, F., Lin, J.-M., 2014. Small 10, 4113–4117.
Oladipupo, S., Hu, S., Kovalski, J., Yao, J., Santeford, A., Sohn, R.E., Shohet, R., Maslov, K., Wang, L.V., Arbeit, J.M., 2011. Proc. Natl. Acad. Sci. USA 108, 13264–13269.
Paige, J.S., Nguyen-Duc, T., Song, W., Jaffrey, S.R., 2012. Science 335, 1194.
Papadopoulos, N., Martin, J., Ruan, Q., Rafique, A., Rosconi, M.P., Shi, E., Pyles, E.A., Yancopoulos, G.D., Stahl, N., Wiegand, S.J., 2012. Angiogenesis 15, 171–185.
Saharinen, P., Eklund, L., Pulkki, K., Bono, P., Alitalo, K., 2011. Trends Mol. Med. 17, 347–362.
Schuler, B., Hofmann, H., 2013. Curr. Opin. Struct. Biol. 23, 36–47.
Vahidi, S., Stocks, B.B., Liaghati-Mobarhan, Y., Konermann, L., 2013. Anal. Chem. 85, 8618–8625.
Wang, N., Mao, S., Liu, W., Wu, J., Li, H., Lin, J.-M., 2014. RSC Adv. 4, 11919–11926.
Wu, J., Chen, Q., Liu, W., Lin, J.-M., 2013. Lab Chip 13, 1948–1954.
Wunderlich, B., Nettels, D., Benke, S., Clark, J., Weidner, S., Hofmann, H., Pfeil, S.H., Schuler, B., 2013. Nat. Protoc. 8, 1459–1474.
Xia, H., Wan, S., Shu, C., Chew, Y., 2005. Lab Chip 5, 748–755.
Xu, Z., Guo, K., Yu, J., Sun, H., Tang, J., Shen, J., Mullen, K., Yang, W., Yin, M., 2014. Small 10, 4087–4092.
Zhang, J., Zhou, R., Inoue, J., Mikawa, T., Ha, T., 2014. Nucleic Acids Res. 42, 3821–3832.